Surface Energies and Thermodynamic Phase Stability in Nanocrystalline Aluminas

J. M. McHale, A. Auroux, A. J. Perrotta, A. Navrotsky*

Corundum, α-Al_2O_3, is the thermodynamically stable phase of coarsely crystalline aluminum oxide, but syntheses of nanocrystalline Al_2O_3 usually result in γ-Al_2O_3. Adsorption microcalorimetry, thermogravimetric analyses, and Brunauer-Emmett-Teller adsorption experiments, coupled with recently reported high-temperature solution calorimetry data, prove that γ-Al_2O_3 has a lower surface energy than α-Al_2O_3 and becomes energetically stable at surface areas greater than 125 square meters per gram and thermodynamically stable at even smaller surface areas (for example, 75 square meters per gram at 800 kelvin). The results are in agreement with recent molecular dynamics simulations and provide conclusive experimental evidence that differences in surface energy can favor the formation of a particular polymorph.

Syntheses of nanocrystalline metal oxides often yield materials structurally different from the thermodynamically stable phase (*1*). Examples are nanocrystalline cubic $BaTiO_3$ (*2*), tetragonal ZrO_2 (*3*), and monoclinic Y_2O_3 (*4*). It is commonly assumed that these metastable structures are adopted in order to lower the total energy of the material through a decrease in surface energy. However, little experimental data on oxide surface energies are available (*5*).

Corundum, α-Al_2O_3, is the thermodynamically stable phase of coarsely crystalline aluminum oxide at standard temperature and pressure conditions, but syntheses of nanocrystalline Al_2O_3 usually result in γ-Al_2O_3 (*6*). In addition, γ-Al_2O_3 can maintain surface areas of ~150 $m^2\ g^{-1}$ at 1073 K (*7*), whereas nanophase α-Al_2O_3 coarsens to values <50 $m^2\ g^{-1}$ at such temperatures. Recently, Blonski and Garofalini (*8*) performed molecular dynamics simulations of various α-Al_2O_3 and γ-Al_2O_3 surfaces. The surface energies for α-Al_2O_3 (*9*) were significantly higher than those of γ-Al_2O_3. According to their data, assuming preferential exposure of the surfaces with lowest energy, γ-Al_2O_3 should become the energetically stable polymorph as specific surface areas exceed ~125 $m^2\ g^{-1}$ (Fig. 1). The thermodynamic stability of γ-Al_2O_3 should be even greater than implied by this energy. As a result of the presence of tetrahedral and octahedral sites in its spinel-type structure, and the fairly random distribution of Al^{3+} and vacancies over these sites, γ-Al_2O_3 has a greater entropy than α-Al_2O_3. The entropy change of the α-Al_2O_3 to γ-Al_2O_3 transition, $\Delta S_{\alpha\rightarrow\gamma}$, is about +5.7 $J\ K^{-1}\ mol^{-1}$ (*10*). Therefore, at room temperature, γ-Al_2O_3 could be thermodynamically stable with respect to α-Al_2O_3 at specific surface areas greater than 100 $m^2\ g^{-1}$, and at 800 K (a temperature typical of a hydroxide decomposition), γ-Al_2O_3 might become thermodynamically stable at specific surface areas greater than only 75 $m^2\ g^{-1}$ (dotted line, Fig. 1).

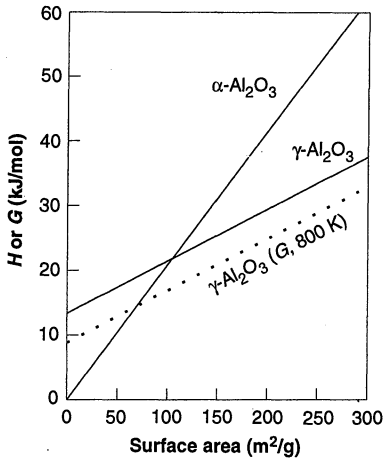

Fig. 1. Calculated enthalpy *H* of alumina polymorphs relative to coarse corundum based on surface energies obtained through molecular dynamics simulations (*8*). The lowest energy relaxed surface and termination [α-Al_2O_3 (0001), C termination; γ-Al_2O_3 (001), A termination] are assumed to be preferentially exposed. The slopes of the lines are the energies for these surfaces as reported in (*8*), 2.04 $J\ m^{-2}$ for α-Al_2O_3 and 0.79 $J\ m^{-2}$ for γ-Al_2O_3. The enthalpy difference between α-Al_2O_3 and γ-Al_2O_3 at zero surface area was taken from (*11*). The dotted line represents the free energy *G* of γ-Al_2O_3 relative to corundum at 800 K.

We have recently explored this possibility by high-temperature solution calorimetry on several samples of nanocrystalline α-Al_2O_3 and γ-Al_2O_3 (*11*). However, the surfaces of the Al_2O_3 were modified by adsorbed H_2O, which could not be completely removed without severe coarsening (especially for α-Al_2O_3). The surface energies of the hydrated polymorphs were nearly equal, indicating that the heat of chemisorption of H_2O is directly proportional to the surface energy of the anhydrous phase [a relation predicted by Cerofolini (*12*)]. Consequently, we could not determine the anhydrous surface energies without accurate knowledge of the heats of chemisorption of H_2O. Herein we report these crucial data.

The heats of chemisorption of H_2O on two samples of γ-Al_2O_3 and two samples of α-Al_2O_3 [prepared according to the methods of Perrotta *et al.* (*13*)] were measured with a Calvet-type microcalorimeter. About 100 mg of alumina was thermally activated under vacuum. The temperature was increased at 2 K min^{-1} to 1023 K, held at 1023 K for 2 hours, and cooled to the adsorption temperature, 303 K. The sample was then exposed to successive small doses of H_2O vapor (0.3 to 3.0 cm^3 per gram of alumina). The residual pressure was increased from 6.67 mPa to 66.7 Pa in 15 to 20 steps. The heat released and volume of H_2O adsorbed were measured at each step. The specific surface areas [measured by means of N_2 adsorption at 77 K by the Brunauer-Emmett-Teller (BET) method], residual H_2O contents [as judged by thermogravimetric analysis (TGA)], and phase purity [measured by powder x-ray diffraction (*7*, *14*)] were determined after the powders were subjected to the outgassing procedure described above.

The TGA revealed that an average 2.6 OH nm^{-2} were not removed under the outgassing conditions. The adsorption data in Fig. 2 are therefore shown as starting at this coverage to account for the presence of these "preadsorbed" hydroxyls. The differential heat of H_2O adsorption on γ-Al_2O_3 (Fig. 2) decreases logarithmically with increasing coverage (Freundlich behavior), which is consistent with previous studies of this material (*15*, *16*). In contrast, the differential heat of H_2O adsorption on α-Al_2O_3 does not show regular logarithmic decay and decreases far less rapidly with increasing coverage. The first 10 OH nm^{-2} adsorbed to the α-Al_2O_3 surface give heats of adsorption that are in excess of −150 kJ mol^{-1}, whereas only the first 5 OH nm^{-2} exceed this value on γ-Al_2O_3. This imbalance indicates a greater number of high-energy sites on α-Al_2O_3 per unit surface area, which are relaxed by the most strongly chemisorbed hydroxyls. This observation is strong evidence that the surface energy of α-Al_2O_3

J. M. McHale and A. Navrotsky, Princeton Materials Institute and Department of Geosciences, Princeton University, Princeton, NJ 08544, USA.
A. Auroux, Institut de Recherches sur la Catalyse, CNRS, 69626 Villeurbanne Cedex, France.
A. J. Perrotta, Aluminum Company of America, ALCOA Technical Center, Alcoa Center, PA 15069, USA.
*To whom correspondence should be addressed. Present address: Department of Chemical Engineering and Materials Science, University of California, Davis, CA 95616, USA. E-mail: anavrotsky@ucdavis.edu

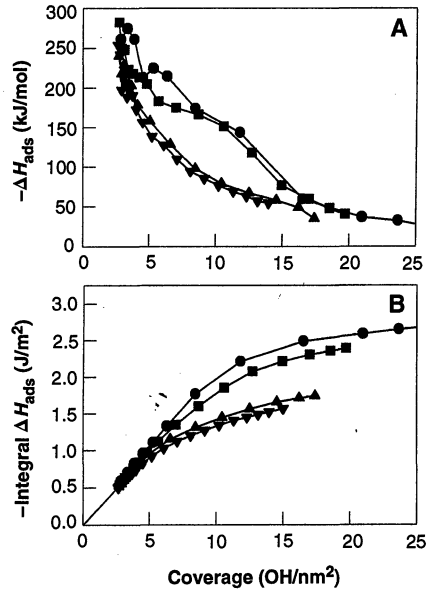

Fig. 2. Differential (**A**) and integral (**B**) heats of chemisorption of H_2O on α-Al_2O_3 [36 m^2 g^{-1} (●), 61 m^2 g^{-1} (■)] and γ-Al_2O_3 [72 m^2 g^{-1} (▲), 161 m^2 g^{-1} (▼)] as a function of hydroxyl coverage.

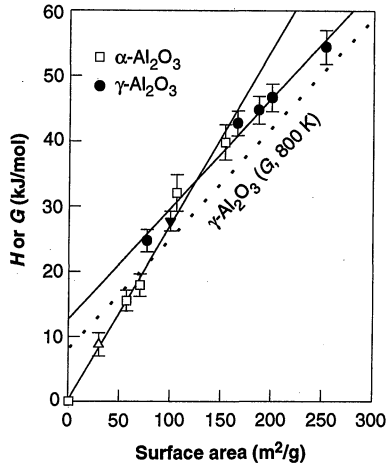

Fig. 3. Enthalpy H of alumina samples relative to coarse-grained α-Al_2O_3 as a function of surface area. The γ-Al_2O_3 (●) lies at lower enthalpy than α-Al_2O_3 (□) when specific surface areas exceed ~125 m^2 g^{-1}. (△) Data for a 30 m^2 g^{-1} sample of α-Al_2O_3 obtained from drop solution and transposed temperature drop calorimetry on diaspore. (▼) Data for a 100 m^2 g^{-1} sample of γ-Al_2O_3 obtained from drop solution and transposed temperature drop calorimetry on boehmite [see (*11*) for details]. The dotted line represents the free energy G of γ-Al_2O_3 relative to corundum at 800 K.

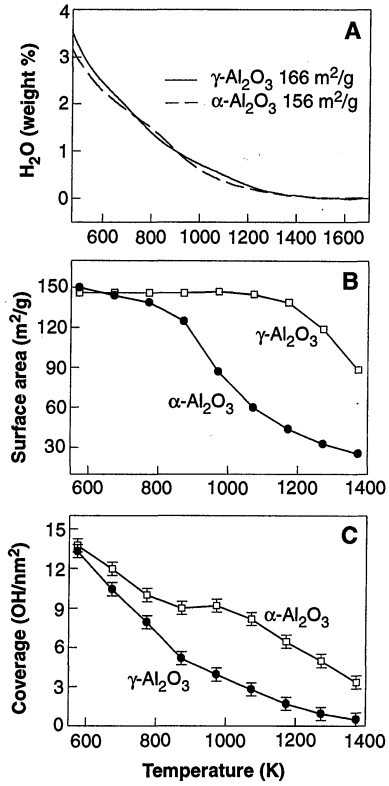

Fig. 4. (**A**) TGA of a 166 m^2 g^{-1} sample of γ-Al_2O_3 and a 156 m^2 g^{-1} sample of α-Al_2O_3. (**B**) Specific surface areas of these samples as a function of temperature (heating rate = 5 K min^{-1}). (**C**) Hydroxyl coverage on the aluminas as a function of temperature.

is higher than that of γ-Al_2O_3.

Assuming that the heat of desorption is the negative of the heat of adsorption (*17*), these data can be used to correct our previously reported calorimetry data on hydrated samples for heat effects due to H_2O desorption. High-temperature drop solution calorimetry had been performed in a Tian-Calvet twin microcalorimeter (*18*) operating at ~979 K, with $2PbO{\cdot}B_2O_3$ as the solvent. The measured heat effect was a combination of the heat content, heat resulting from H_2O removal, and heat of solution of the Al_2O_3. This is represented by reaction 1, where x is the mole fraction of adsorbed H_2O and A_{surf} is the specific surface area. The room-temperature enthalpy difference between the anhydrous nanophase aluminas and coarse corundum can then be obtained through the following thermochemical cycle

$$\alpha \text{ or } \gamma\text{-}Al_2O_3(A_{surf}, 298\ K) + xH_2O \text{ (adsorbed on } Al_2O_3, 298\ K) \rightarrow Al_2O_3 \text{ (dissolved in } 2PbO{\cdot}B_2O_3, 979\ K) + xH_2O \text{ (gas, 979K)} \quad (1)$$

$$H_2O \text{ (adsorbed on } Al_2O_3, 298\ K) \rightarrow H_2O \text{ (gas, 979 K)} \quad (2)$$

$$\alpha\text{-}Al_2O_3 \text{ (corundum, 298 K)} \rightarrow Al_2O_3 \text{ (dissolved in } 2PbO{\cdot}B_2O_3, 979\ K) \quad (3)$$

$$\alpha\text{-}Al_2O_3 \text{ (corundum, 298 K)} \rightarrow \alpha \text{ or } \gamma\text{-}Al_2O_3 \text{ } (A_{surf}, 298\ K) \quad (4)$$

$$\Delta H_4 = -\Delta H_1 + x\Delta H_2 + \Delta H_3 \quad (5)$$

Equation 2 and ΔH_2 represent the correction for heat effects due to adsorbed H_2O, which is the sum of the integral heat of desorption for all of the adsorbed H_2O and the heat content of H_2O vapor between 298 and 979 K.

Before the high-temperature solution calorimetry, the samples were allowed to achieve an equilibrium H_2O content at 295 ± 1 K and 55 ± 2% relative humidity (Table 1). We determined that about 40% of the equilibrium H_2O content was chemisorbed (*11*), which amounted to an average of 16.5 OH nm^{-2} for γ-Al_2O_3 and 17.9 OH nm^{-2} for α-Al_2O_3. The integral heat of chemisorption of H_2O for these coverages can be obtained from the data in Fig. 2B and Table 2. To account for the "preadsorbed" 2.6 OH nm^{-2}, we extrapolated the data below 6 OH nm^{-2} linearly to zero OH nm^{-2} and adjusted by adding 0.490 J m^{-2} to each measured data point, so that the extrapolated line intersected the origin (Fig. 2B). The average integral heat of H_2O chemisorption for these coverages is then −163.7 ± 8.8 kJ (mol H_2O)$^{-1}$ on α-Al_2O_3 and −122.5 ± 4.5 kJ (mol H_2O)$^{-1}$ on γ-Al_2O_3. This value for γ-Al_2O_3 is in good agreement with previous work (*15*, *16*), but no previous data are available for fine-grained α-Al_2O_3. So that we could use these data in our H_2O correction (ΔH_2), the heat content of H_2O vapor between 298 and 979 K, 25.8 kJ mol^{-1}, was added to the negative of these values. For the remaining physisorbed H_2O, the heat of adsorption is (by definition) equal to the heat of condensation of the adsorbate. With our final state as H_2O vapor at 979 K, it contributes 70.1 kJ per mole of physisorbed H_2O to ΔH_2 (*19*). The value of ΔH_2 is then calculated as a weighted average of the contributions from chemisorbed and physisorbed H_2O, yielding ΔH_2 = 118.0 ± 3.5 kJ (mol H_2O)$^{-1}$ for α-Al_2O_3 and 101.5 ± 1.8 kJ (mol H_2O)$^{-1}$ for γ-Al_2O_3.

Through the cycle shown in Eqs. 1 through 5, the enthalpies of the nanophase aluminas relative to coarse grained corundum can now be obtained (Table 1 and Fig. 3). At specific surface areas greater than 125 m^2 g^{-1}, γ-Al_2O_3 lies at lower enthalpy (is more energetically stable) than α-Al_2O_3. The surface energies obtained from the slopes of the least squares fitted lines in Fig. 3 are 2.64 J m^{-2} for α-Al_2O_3 and 1.67 J m^{-2} for γ-Al_2O_3. These values are in agreement with those obtained by computer simulations (*8*, *9*). For example, Blonski and Garofalini (*8*) obtained surface energies (for various exposed surface planes after relaxation) ranging from 2.0 to 8.4 J m^{-2} for α-Al_2O_3 and 0.8 to 2.5 J m^{-2} for γ-

Al_2O_3. The excellent agreement between our calorimetric study and the simulations (*8*, *9*) is evident upon comparison of Figs. 1 and 3, which both show γ-Al_2O_3 becoming energetically stable with respect to α-Al_2O_3 at surface areas $>125 \pm 10$ m^2 g^{-1}. Furthermore, as discussed above, the greater entropy of γ-Al_2O_3 makes this polymorph truly thermodynamically stable with respect to α-Al_2O_3 at surface areas greater than 100 m^2 g^{-1} at room temperature, and greater than only 75 m^2 g^{-1} at 800 K.

To further explore the difference in surface energies and coarsening behavior of the polymorphs, a dynamic study of hydroxyl coverage as a function of temperature was performed on two samples of nearly equal surface area (156 m^2 g^{-1} α-Al_2O_3 and 166 m^2 g^{-1} γ-Al_2O_3). To determine the weight percentage of adsorbed H_2O with increasing temperature, TGA was performed in static air at a heating rate of 5 K min^{-1} to 1773 K. The BET surface area of the aluminas as a function of temperature was then determined from samples heated in Pt crucibles in open air at 5 K min^{-1} to 573, 673, 773, 873, 973, 1073, 1173, 1273, and 1373 K and immediately quenched to room temperature by quick removal from the furnace.

Thermogravimetric analysis of the 166 m^2 g^{-1} γ-Al_2O_3 and 156 m^2 g^{-1} α-Al_2O_3 revealed slight differences in dehydration behavior (Fig. 4A). The loss of H_2O from γ-Al_2O_3 followed a smooth, featureless curve, whereas that of α-Al_2O_3 showed small fluctuations between 673 and 873 K. The coarsening, however, was drastically different for the two polymorphs (Fig. 4B). The α-Al_2O_3 began to coarsen rapidly above 773 K, whereas the γ-Al_2O_3 did not coarsen until above 1173 K. By comparing these two curves, we obtain the coverage of hydroxyl groups on the alumina surfaces as a function of temperature (Fig. 4C). At low temperatures (<773 K), the coverages are fairly similar for both polymorphs. Above 773 K, however, there is a plateau in the coverage of hydroxyl groups on α-Al_2O_3. The α-Al_2O_3 is both rapidly losing H_2O and rapidly coarsening between 773 and 1173 K while apparently maintaining a fairly constant coverage of ~9 OH nm^{-2}. Above 1073 K, the coverage on α-Al_2O_3 gradually decreases. The similarities between the hydroxyl coverages with increasing temperature (Fig. 4C) and differential heats of adsorption (Fig. 2A) are striking. Both sets of data provide a type of energy "spectrum" of the available surface sites and indicate a higher density of high-energy sites on the α-Al_2O_3 surface.

The results reported here explain the relative ease of synthesis of nanocrystalline γ-Al_2O_3 as opposed to nanocrystalline α-Al_2O_3 and have far-reaching implications from phase development in oxide systems to the synthesis and potential application of nanocrystalline materials. As we have shown that surface-energy differences thermodynamically stabilize γ-Al_2O_3 over α-Al_2O_3, the same may indeed be true for cubic $BaTiO_3$ (*20*) and other technologically important materials for which a nanocrystalline morphology would be potentially beneficial in device fabrication. The nanocrystalline tetragonal modification of ZrO_2 results in a significantly lower exothermic heat of immersion in H_2O compared to that of coarse monoclinic ZrO_2, which suggests surface-energy destabilization of monoclinic ZrO_2 as well (*21*). However, a desired phase being metastable as a nanophase with respect to a less desirable polymorph does not preclude its synthesis, as is evidenced by the 154 m^2 g^{-1} α-Al_2O_3 studied in this work and in (*11*). Such materials can still be obtained by well-designed synthetic routes.

Table 1. Summary of sample characterization and high-temperature solution calorimetry data from (*11*), and the enthalpies of these alumina samples obtained when these data are corrected using the new heat of adsorption data: ΔH_1 is the enthalpy of drop solution for samples with equilibrium H_2O content (see Eq. 1) [data taken from (*11*)]; ΔH_4 is the enthalpy relative to corundum (see Eqs. 1 through 5). The phase was determined by x-ray diffraction (XRD). The reported uncertainties are standard deviations.

Phase (XRD)	Surface area (m^2 g^{-1})	x in $Al_2O_3 \cdot xH_2O$ (equilibrium)	ΔH_1 (kJ mol^{-1} $Al_2O_3 \cdot xH_2O$)	ΔH_4 (kJ mol^{-1} Al_2O_3)
α-Al_2O_3	0.83	0.00	106.4 ± 0.5*	0.00
α-Al_2O_3	57	0.210	115.6 ± 1.4	15.6 ± 1.6
α-Al_2O_3	70	0.249	117.7 ± 1.3	18.0 ± 1.7
α-Al_2O_3	106	0.493	132.3 ± 1.9	32.1 ± 2.8
α-Al_2O_3	154	0.617	139.4 ± 0.9	39.9 ± 2.7
γ-Al_2O_3	77	0.271	109.2 ± 1.6	24.8 ± 1.7
γ-Al_2O_3	166	0.693	133.9 ± 1.2	42.8 ± 1.9
γ-Al_2O_3	187	0.719	134.6 ± 1.5	44.8 ± 2.1
γ-Al_2O_3	200	0.804	141.2 ± 1.2	46.7 ± 2.1
γ-Al_2O_3	253	1.060	158.9 ± 1.4	54.5 ± 2.6

*Enthalpy of drop solution of coarse-grained corundum (ΔH_3); see Eq. 3.

Table 2. Results of sample characterization and heat of adsorption experiments. The analysis was done after outgassing in a vacuum at 1023 K for 2 hours. The amount of chemisorbed H_2O is defined as 17.9 OH nm^{-2} for α-Al_2O_3 and 16.5 OH nm^{-2} for γ-Al_2O_3. The corrected integral heat has been adjusted for average residual hydroxyl coverage (2.6 OH nm^{-2}).

Phase	Surface area (m^2 g^{-1})	Residual H_2O (weight %)	Residual coverage (OH nm^{-2})	Integral heat for chemisorbed H_2O (J m^{-2})	Corrected integral heat for chemisorbed H_2O (J m^{-2})	Integral heat for chemisorbed H_2O (kJ mol^{-1})
α-Al_2O_3	61	0.15	1.6	−1.849	−2.339	−157.4
α-Al_2O_3	36	0.19	3.5	−2.036	−2.526	−169.9
						Avg = −163.7 ± 8.8
γ-Al_2O_3	161	0.48	2.0	−1.149	−1.639	−119.4
γ-Al_2O_3	72	0.36	3.3	−1.232	−1.722	−125.7
						Avg = −122.5 ± 4.5

REFERENCES AND NOTES

1. For reviews, see H. Gleiter, *Nanostruct. Mater.* **6**, 3 (1995); R. W. Siegel, *ibid.* **4**, 121 (1994); H. Gleiter, *Prog. Mater. Sci.* **33**, 223 (1989); R. Freer, Ed., *Nanoceramics* (British Ceramic Proceedings 51, Institute of Materials, London, 1993); R. W Siegel, *MRS Bull.* **5**, 60 (1990).
2. S. S. Flaschen, *J. Am. Chem. Soc.* **77**, 6194 (1955).
3. R. C. Garvie, *J. Phys. Chem.* **82**, 218 (1978).
4. G. Skandan *et al.*, *Nanostruct. Mater.* **1**, 313 (1992).
5. A. W. Adamson, *Physical Chemistry of Surfaces* (Wiley, New York, 1990), pp. 313–318.
6. See, for example, G. P. Johnston, R. Muenchausen, D. M. Smith, W. Fahrenholtz, S. J. Foltyn, *J. Am. Ceram. Soc.* **75**, 3293 (1992); P. M. Kumar *et al.*, *Mater. Chem. Phys.* **36**, 354 (1994).
7. K. Wefers and C. Misra, *Alcoa Tech. Pap. 19* (ALCOA, Alcoa Center, PA, 1987).
8. S. Blonski and S. H. Garofalini, *Surf. Sci.* **295**, 263 (1993).
9. The surface energies for α-Al_2O_3 in (*8*) are in fairly good agreement with the results of other simulations. See, for example, W. C. Mackrodt, R. J. Davey, S. N. Black, *J. Cryst. Growth* **80**, 441 (1987); P. W. Tasker, in *Surfaces of Magnesia and Alumina*, W. D. Kingery, Ed. (American Ceramic Society, Columbus, OH, 1984), pp. 176–189; I. Manassidis and M. J. Gillan, *J. Am. Ceram. Soc.* **77**, 335 (1994). No other data are available for γ-Al_2O_3 surfaces.
10. At high temperatures, the $T\Delta S$ term in the free energy may dominate, and a transition from coarse α-Al_2O_3 to γ-Al_2O_3 can be expected at a high enough temperature. No such transition has been detected up to the melting point of α-Al_2O_3, 2327 K [S. Schneider, *Pure Appl. Chem.* **21**, 115 (1970)], but the liquid structure of alumina has been shown to have γ-Al_2O_3 character [that is, tetrahedrally coordinated Al^{3+}, see S. Ansell *et al.*, *Phys. Rev. Lett.* **78**, 464 (1997)]. The lowest temperature at which the

α-Al_2O_3 to γ-Al_2O_3 transition could occur would then be the melting point, so the change in Gibbs free energy ΔG of the α-Al_2O_3 to γ-Al_2O_3 transition would be zero at 2327 K. Taking the enthalpy of the α-Al_2O_3 to γ-Al_2O_3 transition as 13.4 kJ mol^{-1} (*11*), $\Delta S_{\alpha \rightarrow \gamma}$ is 5.7 J K^{-1} mol^{-1}.

11. J. M. McHale, A. Navrotsky, A. J. Perrotta, *J. Phys. Chem. B* **101**, 603 (1997).
12. G. F. Cerofolini, *Surf. Sci.* **51**, 333 (1975).
13. A. J. Perrotta *et al.*, unpublished material.
14. R.-S. Zhou and R. L. Snyder, *Acta Crystallogr. B* **47**, 617 (1991).
15. D. J. Coster, J. J. Fripiat, M. Muscas, A. Auroux, *Langmuir* **11**, 2615 (1995).
16. A. Gervasini and A. Auroux, *J. Phys. Chem.* **97**, 2628 (1993).
17. Hysteresis in adsorption isotherms, which implies a difference between the heats of adsorption and desorption, has been observed [see, for example, A. Bailey *et al.*, *Trans. Faraday Soc.* **67**, 231 (1971)]. However, these phenomena are usually associated with porous adsorbates, where irreversible changes in the pore structure occur upon adsorption. For the relatively nonporous aluminas considered here, the assumption that the heat of adsorption is the negative of the heat of desorption should be valid.
18. A. Navrotsky, *Phys. Chem. Miner.* **2**, 89 (1977).
19. This value was also proved to be accurate for the physisorbed H_2O in our previous study (*11*).
20. B. D. Begg, E. R. Vance, J. Nowotny, *J. Am. Ceram. Soc.* **77**, 3186 (1994).
21. H. F. Holmes, E. L. Fuller Jr., R. B. Gammage, *J. Phys. Chem.* **76**, 1497 (1972).
22. This work was supported by the Aluminum Company of America and NSF grants DMR 95-00812 and DMR 92-15802. We thank I. Aksay for the use of his BET surface-area–measuring equipment.

2 May 1997; accepted 17 June 1997

The Effect of Pressure on Deuterium-Hydrogen Fractionation in High-Temperature Water

T. Driesner*

The pressure dependence of deuterium-hydrogen (D-H) fractionation in water to 500°C and 200 megapascals has been calculated from high-temperature, high-pressure spectroscopic data. Pressure effects have a maximum at the critical temperature of water (20 per mil between 22 and 200 megapascals). Even larger effects are predicted for vaporlike densities from molecular dynamics simulations and molecular orbital calculations. Pressure effects explain many of the large discrepancies in published mineral-water D-H fractionation curves. Possible applications to natural examples include mineral-water isotope geobarometry.

The stable isotopes of oxygen and hydrogen have been the most commonly used geochemical tracers in the study of both fossil and modern fluid-rock interaction processes for more than 30 years (*1*). The most fundamental prerequisite for a successful application of D/H and $^{18}O/^{16}O$ ratios to the reconstruction of fluid sources, fluid quantities, flow directions, or stable-isotope geothermometry is the experimental or theoretical determination of accurate mineral-fluid isotope fractionation factors (*2*).

From statistical mechanical expressions that were derived in the 1940s to calculate equilibrium constants for isotope-exchange reactions between molecular species (*3*), it appeared that the equilibrium constants (and hence, fractionation factors) are a function of temperature only, because for free molecules and solid phases (that is, the favorite objects of theoretical studies and isotope geothermometry, respectively), the vibrational frequencies do not change significantly with pressure. Only for large pressure differences of several gigapascals, shifts of the vibrational frequencies of solids may lead to measurable effects on isotope fractionation (*4*).

However, unlike the case of solids, the vibrational frequencies of water undergo significant changes even at low to moderate pressures at temperatures of interest to many fields of stable-isotope geochemistry (*5*–*9*). Hence, at any given temperature, the fractionation of hydrogen (and oxygen) stable isotopes in systems involving water must be pressure dependent. Here, I quantify the pressure dependence and demonstrate its geochemical importance.

Inspection of the characteristics of the water spectra reveals that the effect of pressure on the D-H isotope fractionation in water may be quantified in a good approximation, even though only parts of the spectrum have been studied at elevated temperatures and pressures. This is possible because only the changes in the reduced partition function ratio of water with increasing pressure at a given temperature need to be calculated, rather than the complete reduced partition function.

The reduced partition function ratio of water can be split into the various contributions by

$$(Q_D/Q_H)_{total} = (Q_D/Q_H)_{stretch}(Q_D/Q_H)_{bend}(Q_D/Q_H)_{lib} \quad (1)$$

with subscripts denoting stretching, bending, and librational modes. Each of the terms is in turn a product of the reduced partition function ratios of several individual bands, for example, for n O-H stretching modes ν:

$$(Q_D/Q_H)_{stretch} = \prod_{\nu=1}^{n} (Q_D/Q_H)_\nu \quad (2)$$

A convenient definition of the pressure effect Γ_p is (*10*)

$$\Gamma_p = (Q_D/Q_H)_{total,P(ref)}/(Q_D/Q_H)_{total,P} \quad (3)$$

with subscript P(ref) denoting a reference pressure and P the pressure of interest. Then, substitution of Eqs. 1 and 2 into Eq. 3 shows that the contributions of all frequency bands that do not shift with pressure will cancel out in the calculation of Γ_p. Hence, only a simple spectral model rather than a full model of the vibrational density of states is required to calculate the pressure effect (*11*).

Using Eq. 3, I calculated the pressure effect to 500°C and 200 MPa. The results indicate a significant pressure effect at all temperatures. The curves in Fig. 1A are smoothed to remove undulations on the order of 1 unit in 1000 ln Γ_p (that is, 1 per mil in δD) resulting from the limited precision of the spectroscopic data. The strongest effects are observed at near-critical temperatures and pressures below about 100 MPa (*12*). This becomes more obvious when the results are plotted as contour lines of equal pressure effect in a P-T diagram (Fig. 1B). Whereas the variations are rather small below 350°C, steep gradients can be seen between 350° and 450°C. This result is not surprising, because most physical properties of water show small gradients in the low-temperature region and steep gradients near the critical point that are reduced at higher temperatures (*13*).

The practical usage of Fig. 1B is that to determine the effect of pressure on a mineral-water equilibrium fractionation factor at a given temperature, the difference between the contour lines at any two pressures has to be added to the fractionation factor when going up in pressure, or subtracted when going down.

To estimate the effect of pressure on the fractionation of the other important pair of stable isotopes in fluid-rock interaction studies ($^{18}O/^{16}O$), I carried out similar calculations using the data of Frantz *et al.* (*5*), and assuming that the O-H stretching fre-

Institut für Mineralogie und Petrographie, Eidgenössische Technische Hochschule–Zentrum, CH-8092 Zürich, Switzerland.

*Present address: Department of Chemical Engineering, The University of Tennessee, 419 Dougherty Building, Knoxville, TN 37996–2200, USA.